Broad and ultra-flattened supercontinuum generation in the visible wavelengths based on the fundamental mode of photonic crystal fibre with central holes*

Yuan Jin-Hui(苑金辉)[a)†], Sang Xin-Zhu(桑新柱)[a)], Yu Chong-Xiu(余重秀)[a)], Xin Xiang-Jun(忻向军)[a)], Shen Xiang-Wei(申向伟)[a)], Zhang Jin-Long(张锦龙)[a)], Zhou Gui-Yao(周桂耀)[b)], Li Shu-Guang(李曙光)[b)], and Hou Lan-Tian (侯蓝田)[b)]

[a)] *Key Laboratory of Information Photonics and Optical Communications (BUPT) of Ministry of Education, Institute of Optical Communication and Optoelectronics, Beijing University of Posts and Telecommunications, Beijing* 100876, *China*

[b)] *Institute of Infrared Optical Fibers and Sensors, College of Information Science and Engineering, Yanshan University, Qinhuangdao* 066004, *China*

(Received 21 August 2010; revised manuscript received 20 January 2011)

By coupling a train of femtosecond pulses with 100 fs pulse width at a repetition rate of 76 MHz generated by a mode-locked Ti: sapphire laser into the fundamental mode of photonic crystal fibre (PCF) with central holes fabricated through extracting air from the central hole, the broad and ultra-flattened supercontinuum (SC) in the visible wavelengths is generated. When the fundamental mode experiences an anomalous dispersion regime, three phases in the SC generation process are primarily presented. The SC generation (SCG) in the wavelength range from 470 nm to 805 nm does not emerge significant ripples due to a higher pump peak power and the corresponding mode fields at different wavelengths are observed using Bragg gratings. The relative intensity fluctuations of output spectrum in the wavelength ranges of 530 nm to 640 nm and 543 nm to 590 nm are only 0.028 and 0.0071, respectively.

Keywords: photonic crystal fibre (PCF), fundamental mode, broad and ultra-flattened supercontinuum, visible wavelengths

PACS: 42.81.–i, 42.81.Bm, 42.81.Cn, 42.81.Dp **DOI:** 10.1088/1674-1056/20/5/054210

1. Introduction

Supercontinuum generation (SCG) in photonic crystal fibre (PCF)[1] is a complicated nonlinear optical phenomenon characterized by a dramatic white-light spectrum.[2] Self-phase modulation (SPM), cross-phase modulation (XPM), four-wave mixing (FWM), soliton effects and Raman shift and coupling with dispersive waves, are the main effects leading to the generation of a broad spectrum in nonlinear PCFs. Generation and application of wide-band SC radiation in different wave-bands by launching short pulses in a PCF with tens of centimeters length have been extensively investigated.[3−12] Since the first observation of SC generation in PCF by Ranka *et al.* in 2000,[13] several experiments and numerical simulations have been performed to investigate the dynamics of SC generation through exciting different order modes in normal and anomalous regimes.[14−17] Dudley *et al.* described the situations in which the second-order mode is predominantly excited.[14] Wadsworth *et al.* reported SC generation with Q-switched pulses in endlessly single-mode PCFs.[18] Tartara *et al.* investigated the third-harmonic generation and four-wave-mixing processes involving energy exchange among different modes.[19] Lee *et al.* observed the generation of femtosecond pulses at 1350 nm by Cerenkov radiation in higher-order modes.[20] Compared with higher-order modes, although the fundamental mode presents a cut-off wavelength below which the attenuation be-

*Project supported by the National Key Basic Research Special Foundation of China (Grant No. 2010CB327605 and 2010CB328300), National High-Technology Research and Development Program of China (Grant No. 2009AA01Z220), the Key Program of Chinese Ministry of Education (Grant No. 109015), the Discipline Co-construction Project of Beijing Municipal Commission of Education (Grant No. YB20081001301), the Open Fund of Key Laboratory of Information Photonics and Optical Communications (Beijing University of Posts and Telecommunications) of Ministry of Education, and the Specialized Research Fund for the Doctoral Program of Beijing University of Posts and Telecommunications, China (Grant No. CX201023).

†Corresponding author. E-mail: yuanjinhui81@163.com

© 2011 Chinese Physical Society and IOP Publishing Ltd

comes very large in SC generation, the better mode quality and lower loss of fundamental mode depress the noise impact, which are significant for steady and effective nonlinear processes in a longer propagation distance, enhancing the degree of spectral broadening and smoothing.

Broad and flattened SC generation in the visible wavelengths extends the wavelengths of light source to specific spectrum region where other lasers are not readily available and plays an important role in the dense wavelength division multiplexing (DWDM) in visible optical communication. Visible radiation from nonlinear PCFs has been demonstrated with a 1550 nm pump,[21,22] however, the visible light is produced in a variety of higher-order modes. In addition, an extremely broad SC extending to visible wavelengths has been demonstrated in soft glass PCFs using femtosecond pulses at 1550 nm,[23] but the flattened degree is not satisfying. Visible SC generations pumped by continuous-wave have recently been reported in Refs. [24]–[27], but significant ripples have emerged due to lower power levels. Here, the experiment of SCG in the fundamental mode of PCF with central holes is shown. A broad and flattened supercontinuum in the visible wavelength regime is generated while the input femtosecond pulse experiences anomalous dispersion regime. Significant ripples are not observed and the relative intensity fluctuations of output spectrum in the wavelength ranges of 530 to 640 nm and 543 to 590 nm are only 0.028 and 0.0071.

2. PCF fabrication

The PCF was preformed by stacking the capillaries with diameters of 0.4 mm, and the capillaries take on the characteristics of higher temperature stabilization, stronger anti-pressure, lower material loss and high-quality optical transmission. Moreover, the coat-tube and capillaries have similar characteristics of temperature, which ensure the inner and outer structures to be kept integration. The optimal drawing velocity and temperature depend on the matching between the steady-state distributions of temperature field of preform and furnace and the temperature of furnace can fall toward the softening temperature of silica glass while the matching condition is achieved. In the process of fabrication, the drawing velocity and temperature were chosen to be 6.5 mm/min and 2145 K. The air pressures of central hole and cladding holes were adjusted through extracting air from central hole or infusing air into cladding holes and the air pressure in central hole was kept lower than that in cladding holes within one standard atmosphere pressure. The central capillary was 8 cm longer than the surrounding ones to extract or infuse air conveniently and prevent the air from leaking into cladding holes or central hole. The diameter of central hole diminished as the air pressure increased in cladding holes or decreased in central hole and the changing slopes were estimated as 0.2 μm per 0.1×10^5 Pa in the air pressure ranges of 1×10^5 to 2×10^5 Pa in cladding holes and 1×10^5 to 0 Pa in central hole.

The scanning electron microscopy (SEM) of the cross-section structure of PCF, which is fabricated through using improved stack and draw technology[28] and extracting air from the central hole, is shown in Fig. 1. Because there are some complicated factors including fluctuations of air pressure, temperature and tension, regarding to the arts and crafts, two air holes are formed in the core region (labeled by circle). Moreover, the cladding holes have deformation to some degree and one of the air-holes in the first ring is much smaller than the others, which can introduce birefringence to a certain extent.

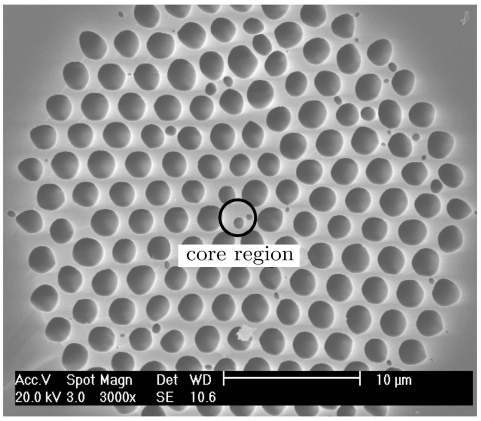


Fig. 1. The amplified cross-section with core region being labeled.

3. PCF properties and experiment

For convenient stimulation, the deformation of cladding holes and core birefringence are neglected and only one central hole is considered. As shown in Fig. 2, the chosen structure parameters are as follows: the average cladding hole radius $r_{\rm clad} = 0.845$ μm, hole to hole pitch $\Lambda = 2.5$ μm, central hole radius

$r_{\rm cen} = 0.4$ μm. Because of larger index contrast between the fibre core and cladding region, the energies of propagation modes are mainly confined in the core region, and the mode effective indices change smaller. Therefore, the established model can well simulate the actual structure.[29] The PCF has an effective mode area of 4.5 μm^2 at 910 nm, corresponding to a nonlinear coefficient $\gamma = 42\ W^{-1} \cdot km^{-1}$. The propagation loss was measured to be 0.08 dB/m at 910 nm by the cut-back method.

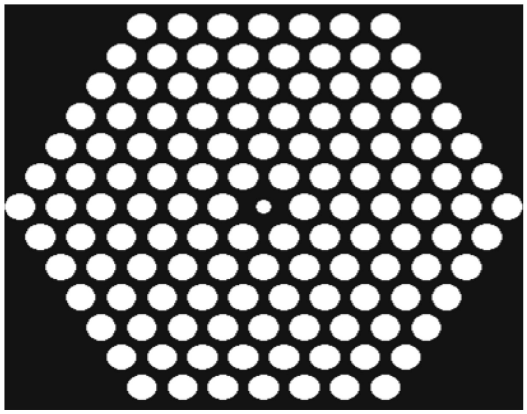


Fig. 2. The established model for simulation.

The multi-pole method (MPM)[30] has been used to analyse the properties of waveguide mode in PCF based on Fig. 2. Figure 3 (a) is the group-velocity dispersion D calculated as a function of wavelength for the fundamental and second-order modes of the PCF with first zero dispersion wavelengths at 918 nm and 765 nm (the second zero dispersion wavelengths are beyond consideration) and the material dispersion is considered from Sellmeyer equation. The dispersion of the fundamental mode is also measured using the Michelson interference method (as labeled by the crossing-line in Fig. 3(a)), where the light source is a SC source with 3 dB bandwidth of 160 nm in the wavelength range from 820 to 980 nm generated by a highly nonlinear fibre and the influence of noise outside the wave-band is eliminated through Fourier-transform and the measured result is more consistent with the simulation result. Because of the dispersion, the profile of the fundamental mode appears more flattened in the near infrared wavelengths compared to the second-order mode, thus it is chosen for SCG. The corresponding transverse field intensity distribution of fundamental mode is shown in Fig. 3 (b). As seen from Fig. 3 (b), it is a doublet of degenerate mode with electric field intensity reaching its maximum at the edge of the central hole and monotonically decreasing with the distance from the central hole.

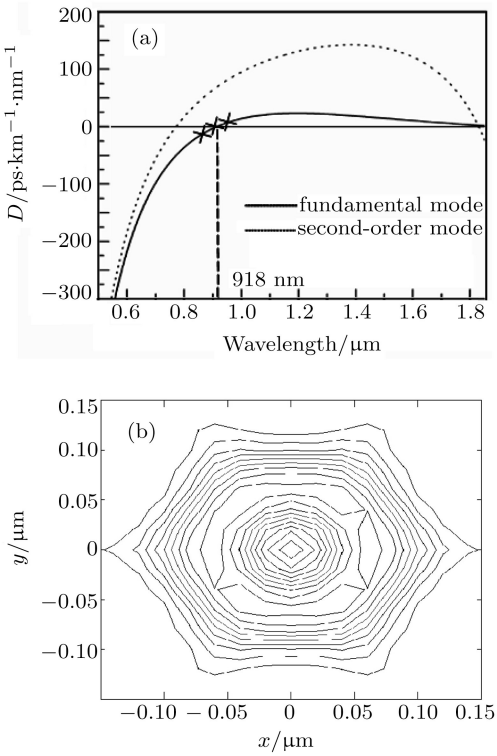


Fig. 3. (a) Group-velocity dispersion calculated as a function of radiation wavelength for the fundamental and second-order modes of the PCF, the crossing-line corresponding to the dispersion value measured using the Michelson interference method. (b) corresponding to the simulated transverse field intensity distribution of fundamental mode.

The configuration of experimental setup is shown in Fig. 4. The light source was a mode-locked Ti: sapphire laser with tunable range from 780 to 980 nm, emitting a 100 fs pulse train at the repetition rate of 76 MHz. A variable attenuator was placed behind the laser to control the input energy and an isolator was inserted to block the back-reflection from the input tip of the fibre into the laser cavity. The polarizer and half-wave plate were used to purify the input polarization. The 40× objective lens with numerical aperture of 0.65 were used for adjusting the input and output efficiencies. The coupling efficiency can be above 65%. CCD1 and CCD2 were used to check the coupling state of input field and observe the output mode field, respectively. By changing the distance between the input tip of the fibre and the lens to adjust the angle exactly between the input beam and the fibre axis (offset pumping technique), the fundamental mode can be selectively excited. The beam went through the first split-beam mirror and one part was coupled into the PCF. The spectral properties of the output radiation were monitored by OSA with a resolution 0.1 nm after the second split-beam mirror.

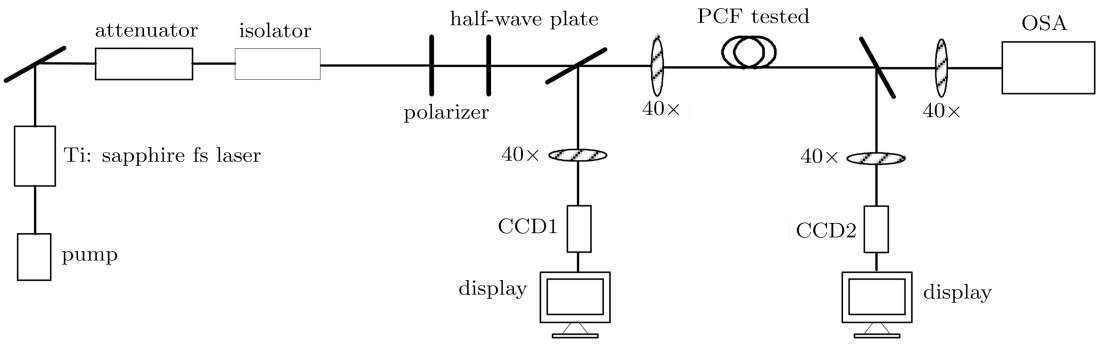


Fig. 4. The configuration of experimental set-up.

4. Results and discussion

The experimental condition and process are carefully optimized. The experiment was carried out by coupling fs pulse with working wavelength of 925 nm (lying in the anomalous dispersion region) and average power of 320 mW (the peak power 15 kW) into the fundamental mode of PCF with a length of 1.85 m (the offset pumping technique). The optimal output spectrum and mode field observed are presented in Figs. 5(a) and 5(b). Figure 5(c) shows the output mode field with the fibre length cut off to be 2/3. Comparing Figs. 5(b) with 5(c), the mode fields show similar distributions, but the lights of sky-blue and weak-green are observed at the edges, showing the influence of fibre length on spectral extending.

In Fig. 5(a), the principle of SCG consists of three basic phases: the initial spectrum broadening and temporal compression based on SPM, the fission of higher order soliton into fundamental soliton components due to higher order dispersion and pulse self-steep effect (SS) and the propagation dynamics of the generated solitons and interactions between the solitons and short wavelength part of SC caused by Raman-type soliton self-frequency shift (SSFS). In the first phase, when the fs pulse is launched near the zero dispersion wavelength of fundamental mode of PCF and experiences anomalous dispersion, the SPM is viewed as four-wave mixing of different frequency components belonging to the broad spectrum of radiation. Frequency components near the zero dispersion wavelength then serve as a pump for phase-matched FWM, which depletes the spectrum of radiation around zero dispersion wavelength and transfer the radiation energy to the region of normal (< 918 nm) and anomalous (>918 nm) dispersion. In the second phase, owing to the simulated Raman Scattering, the shorter wavelength components are gradually converted into longer ones and the Raman spectral components are generated at the longer wavelength side. When the negative dispersion and SPM interplay, the higher order solitons are formed due to stronger pump power in anomalous dispersion region and they will break up into some fundamental solitons associated with higher-order dispersion and SS. In the third phase, on one hand, the fundamental solitons constantly shift to the longer wavelength due to SSFS and this process is the Raman-type amplification of the long wavelength part of the pulse spectrum at the expense of the depletion of its short wavelength wing. On the other hand, the high-order dispersion induces instabilities of these solitons and the emission of dispersive waves referred to as Cherenkov radiations are generated at the shorter wavelengths based on the phase matching between the red-shift solitons and blue-shift waves.[12] Because the soliton group velocity continuously decreases during the Raman shifting process, the XPM traps the dispersive waves, leading to blue-shift up to wavelengths that make the group velocities of two waves equal. In the time domain, the optical pulses in the normal dispersion region are trapped by the soliton pulses in the anomalous dispersion region and then the two pulses co-propagate along the fibre. As the solitons progressively shift towards longer wavelengths, the dispersive waves experience XPM and are widened constantly. As shown in Fig. 5 (a), the experimental result agrees well with the predictions of GNSE simulations. This process will move the blue edge towards shorter wavelength and generate broad and flattened visible continuum as long as the solitons continuously shift towards longer wavelength. The intrinsic loss at near-infrared wavelengths and SS effect are considered to be the primary limiting factors.

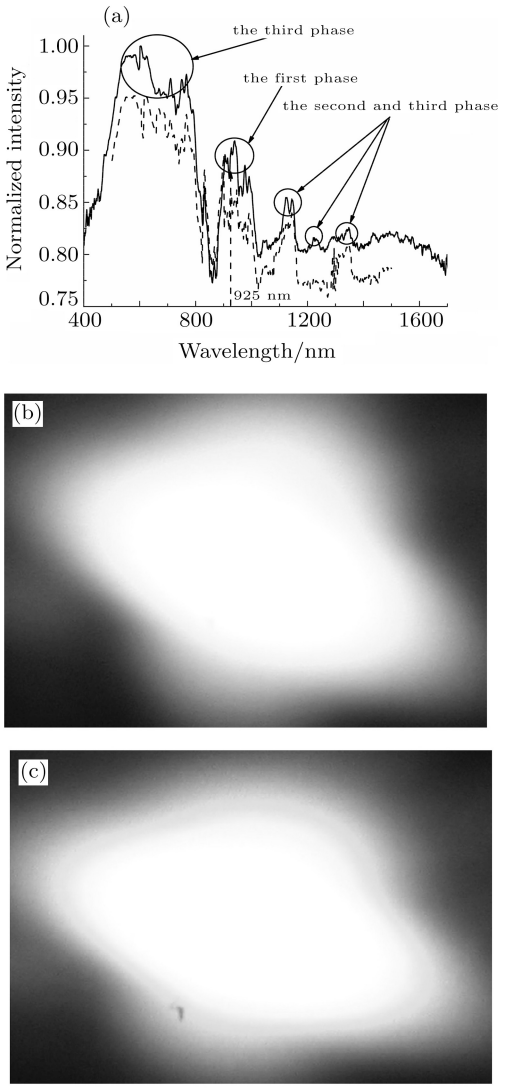


Fig. 5. The normalized intensity of output spectrum from 400 nm to 1700 nm (a), the corresponding output mode field (the white light at the centre and sky-blue light at the edge) observed with a fibre length of 1.85 m (b), and the output mode field (the white light at the centre and weak-green light at the edge) with 2/3 length (c). The dash line in (a) shows the numerical solution of the generalized nonlinear Schrödinger equation (GNSE) in the wavelength range of from 500 nm to 1500 nm and the circles associated with arrowheads indicate the different evolution phases in the SCG process.

Figure 6(a) shows the output SC spread by the Bragg gratings with different central wavelengths. The normalized intensity of output spectrum from 400 to 850 nm is presented in Fig. 6(b) and the inserts show the output fields at given wavelengths. As shown in Fig. 6(b), the 3 dB bandwidth output spectrum in the range from 470 nm to 805 nm does not emerge significant ripples due to higher pump peak power (15 kW), indicating significant walk-off in time domain of adjacent spectrum components, instead of significant overlap in the time domain of the SCG in the case of lower pump peak power. Especially, the spectrum feature in the wavelength range from 530 nm to 640 nm is much broader and smoother, as shown in Fig. 7.

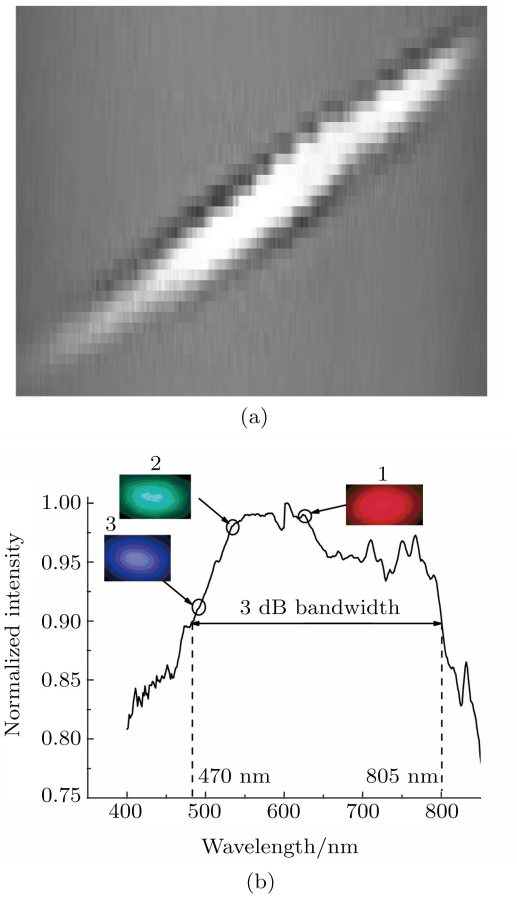


Fig. 6. (colour online) (a) The output SC spread by the Bragg gratings, showing different colours (red, green and blue light). (b) The normalized spectrum intensity from 400 nm to 850 nm and the corresponding 3 dB bandwidth is from 470 nm to 805 nm (as indicated by horizontal and vertical solid lines). Inserts show the corresponding mode fields with red (1), green (2) and blue (3) lights at given wavelengths, respectively.

At the short wavelength, the soliton trapping of dispersive waves is the dominant mechanism and the FWM-like interaction between solitons and DWs leads to the continuous blue shift of the trapped pulses and enhances the flattened and smooth degree. In Fig. 7(a), the flattened SC in the wavelength range from 530 nm to 640 nm is shown, the maximal and minimal normalized intensities are 1.0 at 607 nm and 0.972 at 640 nm and the relative intensity fluctuation (defined as $|I_{\max} - I_{\min}|/I_{\max}$) is only 0.028. The Fig. 7(b) shows the output spectrum from 543 to 590 nm labeled by circle in Fig. 7(a), and the corresponding maximal and minimal normalized intensities are 0.9915 at 585 nm and 0.9845 at 590 nm, the relative intensity fluctuation being only 0.0071.

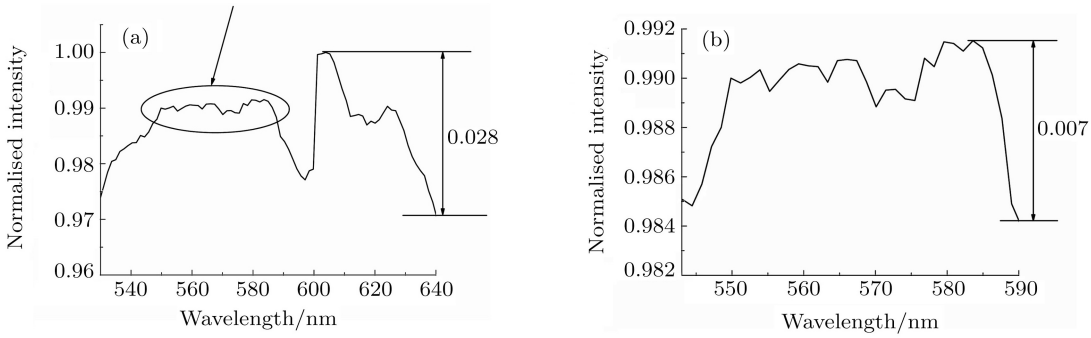


Fig. 7. (a) The normalized spectrum intensity from 530 nm to 640 nm, (b) the output spectrum from 543 nm to 590 nm corresponding to the region labeled by circle.

5. Conclusions

In summary, the PCF with central holes is fabricated through extracting air from the central hole and the broad and flattened SC in the visible wavelengths is generated by coupling a train of femtosecond pulses into the fundamental mode. The SC from 470 nm to 810 nm is mainly considered and the ultra-flattened SCs in the wavelength ranges from 530 nm to 640 nm and 543 nm to 590 nm are shown. Such SC provides a light source with specific spectrum region where other lasers are not readily available and is the essential building block in state-of-the-art SC microscope system. Especially, it is also important for WDM in high speed optical communication in the visible wavelengths. Our further works are primarily concentrated on optimizing the fibre design, choosing the appropriate length, optimizing the parameters of experimental system to generate much broader and flatter SC in the ultraviolet and mid-infrared wavelengths.

References

[1] Dudley J M, Genty G and Coen S 2006 *Rev. Mod. Phys.* **78** 1135
[2] Alfano R R and Shapiro S L 1970 *Phys. Rev. Lett.* **24** 584
[3] Foster M A, Dudley J M, Kibler B, Cao Q, Lee D, Trebino R and Gaeta A L 2005 *Appl. Phys.* B **81** 363
[4] Kibler B, Dudley J M and Coen S 2005 *Appl. Phys.* B **81** 337
[5] Kolesik M, Wright E M and Moloney J V 2004 *Appl. Phys.* B **79** 293
[6] McConnell G and Riis E 2004 *Appl. Phys.* B **78** 557
[7] Nicholson J W, Abeeluck A K, Headley C, Yan M F and Jørgensen C G 2003 *Appl. Phys.* B **77** 211
[8] Town G E, Funaba T, Ryan T and Lyytikainen K 2003 *Appl. Phys.* B **77** 235
[9] Liu W H, Song X Z, Wang Y S, Liu H J, Zhao W, Liu X M, Peng Q J and Xu Z Y 2008 *Acta Phys. Sin.* **57** 917 (in Chinese)
[10] Chen Y Z, Li Y Z, Qu G and Xu W C 2006 *Acta Phys. Sin.* **55** 717 (in Chinese)
[11] Duan Z L Li Y F Liu H J Liu W H Peng Q J Wang Y S Xu Z Y and Zhao W 2006 *Acta Phys. Sin.* **55** 1815 (in Chinese)
[12] Liu B W, Hu M L, Fang X H, Li Y F, Chai L ,Wang C Y, Tong W J, Luo J, Voronin A A and Zheltikov A M 2008 *Opt. Express* **16** 14987
[13] Ranka J K, Windeler R S and Stentz A J 2000 *Opt. Lett.* **25** 25
[14] Dudley J M, Provino L, Grossard N, Maillotte H, Windeler R S, Eggleton B J and Coen S 2002 *J. Opt. Soc. Am.* B **19** 765
[15] Gaeta A 2002 *Opt. Lett.* **27** 924
[16] Cristiani I, Tediosi R, Tartara L and Degiorgio V 2004 *Opt. Express* **12** 4366
[17] Genty G, Lehtonen M, Ludvigsen H and Kaivola M 2004 *Opt. Express* **12** 124
[18] Wadsworth W, Joly N, Knight J C, Birks T A, Biancalana F and Russell P S J 2004 *Opt. Express* **12** 299
[19] Tartara L, Cristiani I, Degiorgo V, Carbone F, Faccio D, Romagnoli M and Belardi W 2003 *Opt. Commun.* **215** 191
[20] Lee J H, Hove J V, Xu C, Ramachandran S, Ghalmi S and Yan M F 2007 *Opt. Lett.* **32** 1053
[21] Efimov A, Taylor A, Omenetto F, Knight J C, Wadsworth W and Russell P St J 2003 *Opt. Express* **11** 2567
[22] Efimov A, Taylor A, Omenetto F, Knight J C, Wadsworth W and Russell P S J 2003 *Opt. Express* **11** 910
[23] Ravi V V, Kumar K, George A K, Reeves W H, Knight J C, Russell P St J, Omenetto F G and Taylor A J 2002 *Opt. Express* **10** 1520
[24] Kudlinski A and Mussot A 2008 *Opt. Lett.* **33** 2407
[25] Cumberland B A, Travers J C, Popov S V and Taylao J R 2008 *Opt. Lett.* **33** 2122
[26] Cherif R, Zghal M, Tartara L and Degiorgio V 2008 *Opt. Express* **16** 2147
[27] Frosz M H, Moselund P M, Rasmussen Per D, Thomsen C L and Bang O 2008 *Opt. Express* **16** 21076
[28] Zhou G Y, Hou Z Y and Hou L T 2006 *Appl. Opt.* **45** 1
[29] Wang W, Gao F, Hou L T and Zhou G Y 2008 *Chin. Phys. Lett.* **25** 2055
[30] White T P, Kuhlmey B T, McPhedran R C, Maystre D, Renversez G, de Sterke C M and Botten L C 2002 *J. Opt. Soc.* B **19** 2322